Supporting Information

Hierarchical Metal-Organic Framework Nanoflowers for Effective CO$_2$ Transformation Driven by Visible Light

Shuquan Zhang,[a] Lina Li,[a] Sangen Zhao,[a] Zhihua Sun,[a]   Maochun Hong[ab] and Junhua Luo[a*]

[a]*Key Laboratory of Optoelectronic Materials Chemistry and Physics, Fujian Institute of Research on the Structure of Matter, Chinese Academy of Sciences, Fuzhou, Fujian，350002, P.R. China.*

[b]*State Key Laboratory of Structural Chemistry, Fujian Institute of Research on the Structure of Matter, Chinese Academy of Sciences, Fuzhou, Fujian，350002, P.R. China.*

*To whom correspondence should be addressed: E-mail: jhluo@fjirsm.ac.cn; Fax: (+86) 591-63173127; Tel: (+86) 591-63173126.

Experimental Section

Materials and Measurements: All reactants were reagent grade and used as purchased without further purification. Elemental analyses for C, H, N were carried out on a German Elementary Vario EL III instrument. The FT-IR spectra were performed on a Nicolet Magna 750 FT-IR spectrometer using KBr pellets in the range of 4000-400 cm^{-1}. The thermal decomposition behavior was analyzed by thermogravimetric analysis-mass spectrometry (TGA-MS) using a NETSCH STA-449C thermoanalyzer coupled with a NETSCH QMS403C massspectrometer. The power X-ray diffraction (PXRD) patterns were collected by a Rigaku DMAX2500 X-ray diffractometer using Cu Kα radiation (λ = 0.154 nm). Fluorescent analysis was performed on an Edinburgh Instruments FLS920 spectrofluorimeter equipped with both continuous (450 W) and pulse xenon lamps. UV/visible absorbance was collected in the solid state at room temperature on a Perkin-Elmer Lambda 650S UV/vis spectrometer equipped with Labsphere integrating over the spectral range 300-800 nm using $BaSO_4$ as reflectance standards. SEM analyses were performed using Phenom G2 pro desktop scanning electron microscopy (SEM) and JSM-6700F SEM equipped with an Oxford-INCA energy dispersive X-ray (EDX) spectroscopy. The ^{13}C NMR spectra were measured using a Bruker AVANCE 400 spectrometer under the following conditions: acquisition time 2 s; 10500 times integration. Nitrogen adsorption measurements were performed in the Accelerated Surface Area and Porosimetry 2020 (ASAP2020) System.

Synthesis of the metalloligand [Ru(H$_2$dcbpy)$_3$]·Cl$_2$. [Ru(H$_2$dcbpy)$_3$]·Cl$_2$ was synthesized by following the published procedure.[1] $RuCl_3·3H_2O$ (50 mg) and H_2dcbpy (140 mg) were placed in a 23 mL teflon-lined stainless steel container, where 1 mL of HCl (37%) and 2 mL of water were added. The mixture was heated at 200 ℃ for 4 h and cooled to room temperature. The dark red block crystals were filtered off and washed a few times with water. Yield: 152 mg (83%).

Synthesis bulk crystals and flower-like hierarchical nanostructure of Ru-MOF. A mixture of [Ru(H$_2$dcbpy)$_3$]·Cl$_2$ (0.005 mmol, 5 mg) and $Cd(ClO_4)_2·6H_2O$ (0.024 mmol, 10 mg) was dissolved in 10 mL DMF/H_2O solution in a 20 mL vial, and then was added small amount of acid. The resulting solution was heated for 1.5 days at 100 °C. The product was obtained as bulk crystals (yield 68% based on [Ru(H$_2$dcbpy)$_3$]·Cl$_2$). The complete formula of the {Cd$_2$[Ru(dcbpy)$_3$]·12H$_2$O}$_n$ for **Ru-MOF** was obtained by the combination of TGA-MS and elemental analysis (Figure S4).

Anal. Calcd for $C_{36}N_6O_{24}H_{42}RuCd_2$: C, 34.08; H, 3.34; N, 6.62%. Found: C, 34.01; H, 3.39; N, 6.81%. IR (cm-1): 3396(m, br), 3072(w), 1598(s), 1542(s), 1371(s), 1234(w), 913(w), 780(m), 702(m).

The flower-like hierarchical nanostructure of **Ru-MOF** was obtained through similar reaction condition to that of bulk crystals except that the reactant concentration was reduced to 1/5 of original level. After 10 hours reaction, the product was obtained as red precipitate. The red precipitate was collected by centrifugation and washed with methanol twice. After drying in air, the yield based on $[Ru(H_2dcbpy)_3]\cdot Cl_2$ was 77%. Elemental Analysis: Anal. Calcd: C, 34.08; H, 3.34; N, 6.62%. Found: 34.35, H, 3.25, N, 6.77%.

Photocatalytic reaction: The visible-light induced photocatalytic CO_2 reduction was performed in a 100mL Schlenk tube with as-prepared samples. Photocatalyst (40 mg) enclosed in the tube was treated with vacuum then purged with CO_2 for several times. At the same time, a mixture of MeCN and TEOA (60 mL, 20/1 v/v) was degassed by CO_2 to remove dissolved O_2 and then injected into the reaction tube. The reaction was performed under the irradiation of a 500 W Xe lamp with a UV-cut filter to remove all wavelengths lower than 420 nm and an IR-cutfilter to remove all wavelengths longer than 800 nm. The $HCOO^-$ formed was detected by ion chromatography (881 Compact IC pro, Metrosep) with Metrosep A supp 5 250/4.0 column. The column temperature was maintained at 303 K. The eluent is the aqueous solution of 3.2 mM Na_2CO_3 and 1.0 mM $NaHCO_3$.

X-ray crystallography and structural resolving

The structure data of **Ru-MOF** was collected on an Agilent Supernova CCD diffractometer equipped with a graphite-monochromated Cu Kα radiation (λ = 1.54184 Å) at 100K. The structures was resolved by the direct method and refined by full-matrix least-squares fitting on F^2 by SHELX-97.[2] All non-hydrogen atoms were refined with anisotropic thermal parameters. The hydrogen atoms were located at geometrically calculated positions and refined by riding. In addition, SQUEEZE subroutine of the PLATON software suite[3] was applied to remove the scattering from the highly disordered guest molecules. The resulting new HKL4 files were used to further refine the structures. Crystallographic data and structure refinement parameters for **Ru-MOF** are summarized in Table S1. Selected bond lengths and bond angles are listed in Table S2. More details on the crystallographic studies as well as atomic displacement parameters are given in Supporting Information as CIF files. Crystallographic data for the structure reported in this paper have been

deposited in the Cambridge Crystallographic Data Center with CCDC reference number 965739.

Thermogravimetric Analysis (TGA-MS)

To study the thermal stability and determine the compose of the guest molecules of **Ru-MOF**, TGA coupled with QMS analysis was performed on bulk polycrystalline samples and microparticles under a N_2 atmosphere with a heating rate of 10 °C min^{-1} in the temperature range 30-800 °C. A total loss of 15.3% and 14.1% was observed for bulk samples and microparticles of **Ru-MOF** in the temperature range of 30−200 °C (cal: 17.0%), and mass fragment 17 m/z corresponding to H_2O is also observed in the range 30−200 °C. The value of observed weight loss was slightly small than calculated one, which may be attributed to the loss of a small portion of guest molecules before TGA measurement. This phenomenon is easier to happen in a nanoscale porous metal-organic material. The decomposition of the residue of both samples was observed at about 290 °C. And in the whole temperature region, no mass fragment 73 m/z is observed indicating no DMF molecules in this structure (Fig. S5).

Possible formation mechanism for the nanoflowers of Ru-MOF

In order to understand the formation process of the microflowers, we carried out concentration-dependent experiments during which samples were collected from the reaction mixture with different concentrations after 5 hours reaction. As shown in Figure S7a, at a high reactant concentration, the sample was mainly composed of bulk laminar crystals of **Ru-MOF**, the dimensions of which can reach ca. 100 μm in width and ca. 10 μm in thickness. Meanwhile, although some smaller laminar crystals could also be observed, they were almost monodisperse and did not aggregate to hierarchical structure. As reactant concentration reduced (Figure S7b), the main product were also laminar structure, but the dimensions of them are obviously decreased (15-40 μm in width and less than 5 μm in thickness). It is noticeable that, in this reaction condition, many very thin laminas with hundreds of nanometers in thickness appeared, some of which grew on the surface of another one to form the rudiment of flower-like hierarchical structure. When the concentration of reactant was reduced to 60% (or 40%) of original one, the size of laminae further decreased to less than 10μm in width and about dozens of nanometers in thickness (Figure S7c). Meanwhile, most of nanoflakes attached to each other and self-assembled to flower-like microspheres. Whereas, a few nanoflakes were still single laminas or simply aggregated as multilayers. The morphology of the

microflowers evolves further when the reactant concentration was decreased to 20% of original one. As shown in Figure S7d, the nanoflakes maintained their dimensions and all of them were assembled to flower-like microspheres. From the above mentioned experiment results, we can temporary suppose that the morphology of **Ru-MOF** is concentration controlled.

A possible formation mechanism for the flower-like hierarchical microsphere is schematically illustrated in Figure S6e. At the preliminary stage of reaction, along with the chemical reaction, product generated gradually from the solution and still dissolved in it. When the concentration of product kept increasing and was in the area between the saturation and the supersaturation curves (located in the metastable zone, Figure S9), MOF nanoflakes nucleated from the solution by thermal fluctuations. Thermal fluctuations in extrinsic thermodynamic variables are present in all systems at equilibrium, but are proportionally more significant in nanoscale systems.[4] And, at this time, equilibrium is set up between the spontaneous nucleation and dissipation of nanosheet seeds. Moreover, it is noticeable that a new nanosheet tended to nucleate on an existing nanosheet surface due to its high surface energy. When the reaction is proceeding, the reaction solution with different concentrations will lead to different growth process of MOF nanoflakes. A rich reaction solution, just like the situation of Figure S6a, will generate large amount of product resulting in a very high product concentration at the moment which is far above the supersolubility curves (Figure S9). As a result, the balance of nucleation and dissipation was broken and nucleated rate of new nanoflakes was considerably lower than the growing rate of exiting nanoflakes. MOF crystals grew rapidly and continuously until the solution concentration fell to the saturation line. This process, which is tentatively supposed to be dominated by thermodynamics, would finally lead to the formation of microscale and even millimeter-sized bulk crystals. However, a dilute reaction solution, the case of Figure S7d, may more likely to exhibit a kinetic process for the growth of nanoflakes. In this case, because of the low reactant concentration, the amount of the product cannot support the rapid growth of nanoflakes. Therefore, it is benefit to the development of new nanoflakes. As a result, although the equilibrium was also broken, no bulk crystals were obtained, and instead, nanosheet seeds grew outwards and aggregated spontaneously to form flower-like hierarchical nanostructures. The formation of flower-like microsphere may assemble to a ZnS flower-like structure reported by Huang and coworkers.[5] At the same time, we have tried to trace the formation of flower-like hierarchical nanostructures by time-dependent experiments (Figure S10), however, unfortunately,

this process is too fast to be accurately verified with the imaging data. Further work is underway to investigate the detail of the self-assembly growth mechanism.

Table S1. Crystallographic data and structure refinement details for **Ru-MOF**

complexe	Ru-MOF
framework formula	$C_{36}N_6O_{12}H_{18}RuCd_2$
formula weight	1052.44
crystal system	Monoclinic
space group	$C2/c$
a (Å)	19.8070 (5)
b (Å)	15.3580 (3)
c (Å)	23.9322 (6)
α (°)	90
β (°)	116.709 (3)
γ (°)	90
V(Å^3)	6503.3 (3)
Z	4
T/K	100(2)
D_C (g cm^{-3})	1.075
μ(mm^{-1})	7.41
F(000)	2048
θ range (°)	3.8–75.5°°
Collected reflections	18533
unique reflections	6564
parameters	258
Gof on F^2	1.236
$R_1{}^a$ ($I > 2\sigma(I)$)	0.0299

$wR_2{}^b$ (all data)		0.0850	

$^a R_1 = \Sigma||F0| - |Fc||/\Sigma|F0|.$ $^b wR2 = [\Sigma w(Fo^2 - Fc^2)^2 /\Sigma w(F0)^2]^{1/2}.$

Table S2. Selected Bond Lengths (Å) and Bond Angles (°) for **Ru-MOF**

Cd1—O3	2.226 (2)	Ru1—N3	2.044 (2)
Cd1—O1^i	2.229 (4)	Ru1—N3^v	2.044 (2)
Cd1—O6^{ii}	2.242 (3)	Ru1—N2^v	2.052 (2)
Cd1—O5^{iii}	2.254 (3)	Ru1—N2	2.052 (2)
Cd1—O4^{iv}	2.259 (3)	Ru1—N1	2.062 (3)
Cd1—O2^i	2.507 (4)	Ru1—N1^v	2.062 (3)
O3—Cd1—O1^i	130.43 (15)	N3—Ru1—N3^v	78.67 (13)
O3—Cd1—O6^{ii}	86.64 (12)	N3—Ru1—N2^v	98.08 (10)
O1^i—Cd1—O6^{ii}	99.52 (19)	N3^v—Ru1—N2^v	88.68 (10)
O3—Cd1—O5^{iii}	91.36 (12)	N3—Ru1—N2	88.68 (10)
O1^i—Cd1—O5^{iii}	105.10 (19)	N3^v—Ru1—N2	98.08 (10)
O6^{ii}—Cd1—O5^{iii}	149.06 (16)	N2^v—Ru1—N2	171.29 (14)
O3—Cd1—O4^{iv}	151.45 (10)	N3—Ru1—N1	98.31 (11)
O1^i—Cd1—O4^{iv}	77.46 (14)	N3^v—Ru1—N1	175.76 (10)
O6^{ii}—Cd1—O4^{iv}	81.82 (14)	N2^v—Ru1—N1	94.72 (10)
O5^{iii}—Cd1—O4^{iv}	85.50 (12)	N2—Ru1—N1	78.79 (10)
O3—Cd1—O2^i	81.40 (13)	N3—Ru1—N1^v	175.76 (10)
O1^i—Cd1—O2^i	49.60 (15)	N3^v—Ru1—N1^v	98.31 (11)
O6^{ii}—Cd1—O2^i	106.97 (19)	N2^v—Ru1—N1^v	78.79 (10)
O5^{iii}—Cd1—O2^i	103.22 (17)	N2—Ru1—N1^v	94.72 (10)
O4^{iv}—Cd1—O2^i	126.96 (13)	N1—Ru1—N1^v	84.85 (16)

Symmetry codes: (i) 3/2-x, 3/2-y, 1-z; (ii) 1/2+x, 1/2+y, z; (iii) 3/2-x, 1/2-y, 1-z; (iv) 2-x, 1-y, 1-z; (v) 1-x, y, 1/2-z.
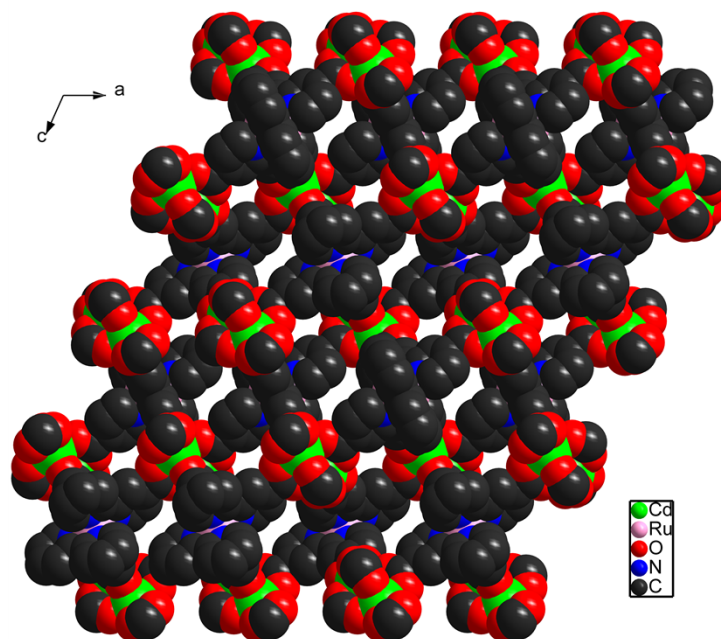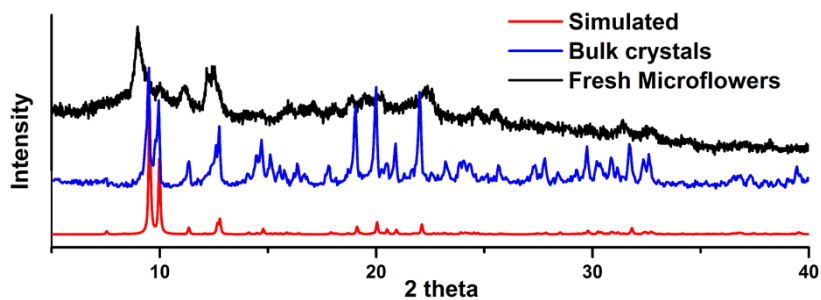
Figure S1. The space-filling mode of **Ru-MOF**, showing the small channel along *b* axis.
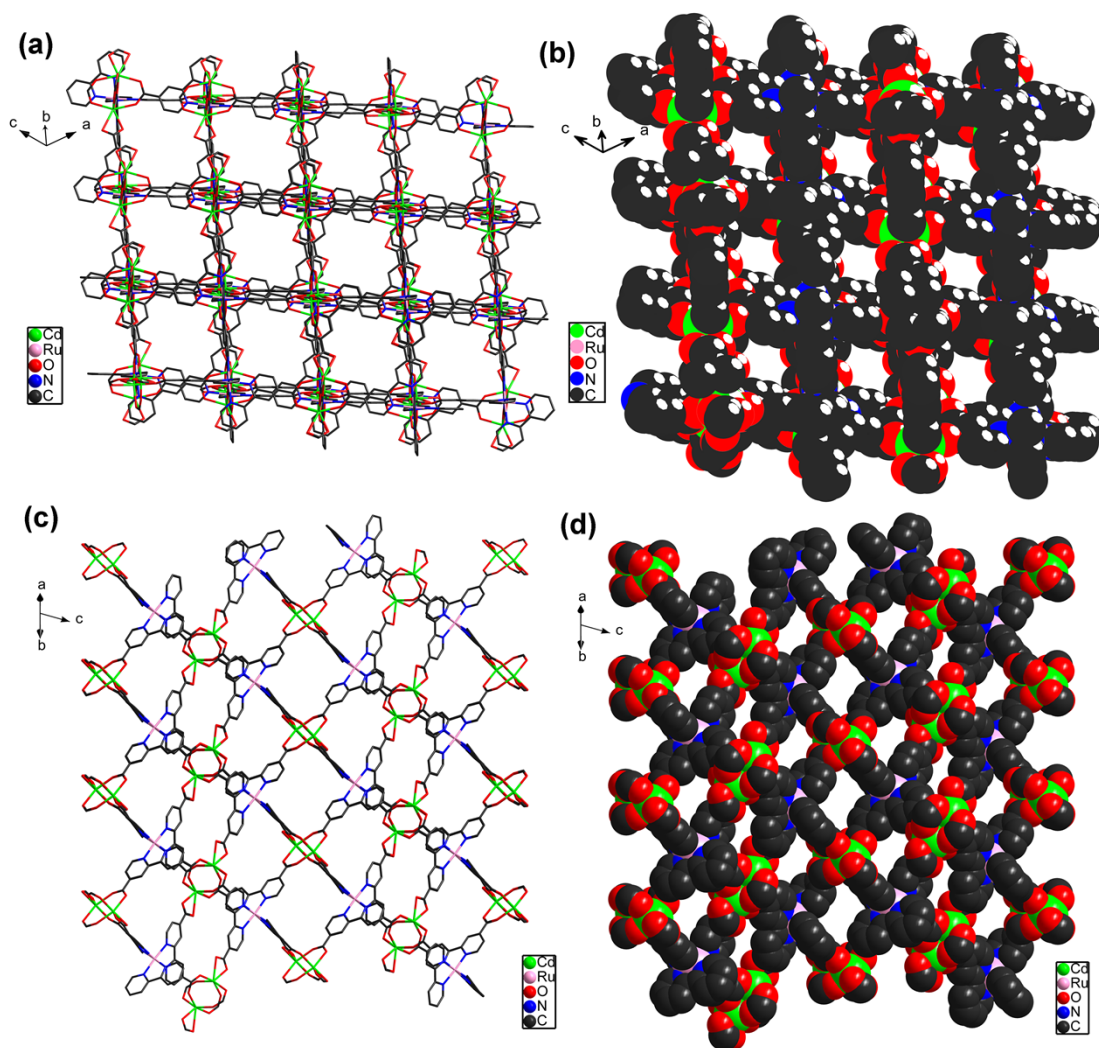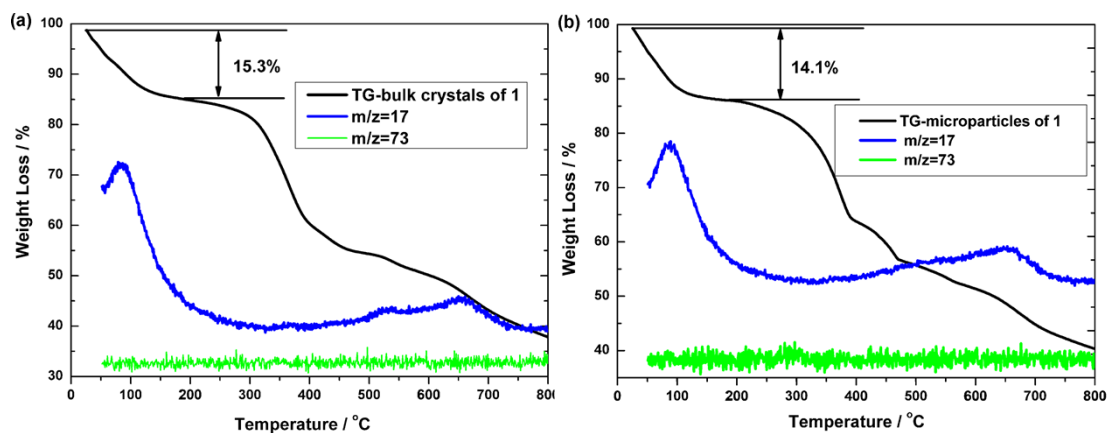

Figure S2. (a), (b) Stick and space-filling mode showing the open channels along [5,-12.3, 8.9]
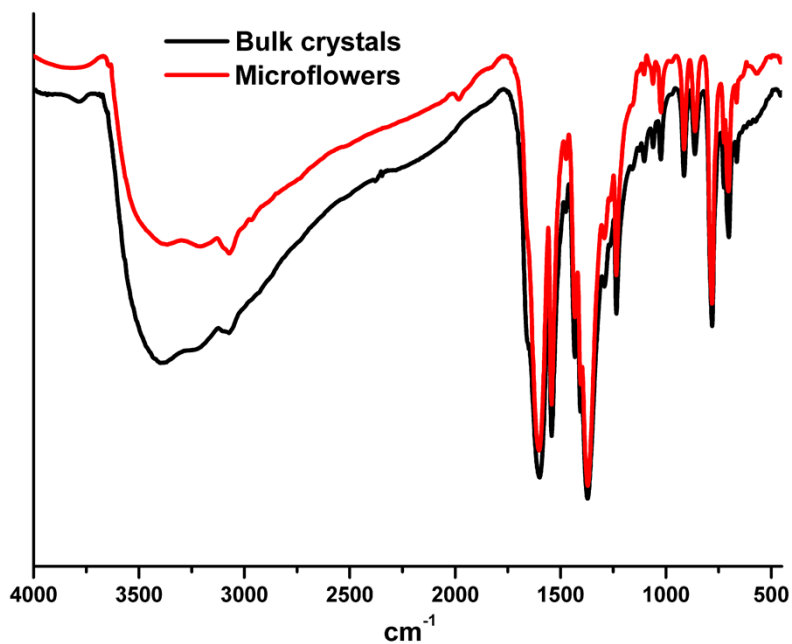
direction; (c), (d) Stick and space-filling mode showing the open channels along [15.5 9.8 -7.5] direction.
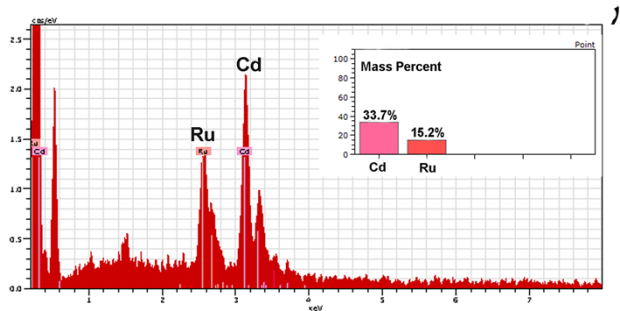

Figure S3. PXRD patterns of simulated, as-synthesized bulk crystals and fresh flower-like micro particles of **Ru-MOF**


Figure S4. TGA coupled with QMS analyses of bulk crystals and microparticles of **Ru-MOF** with ion current signal for m/z = 73 (green) and m/z = 17 (blue).

Figure S5. IR spectra of bulk crystals and flower-like micro particles of **Ru-MOF**

Figure S6. The EDX image of nanoflowers of **Ru-MOF**, indicating that the molar ratio of Cd(II) to Ru(II) ions in the nanoflowers is 2.006:1, which perfectly matches the crystal structure of **Ru-MOF**.
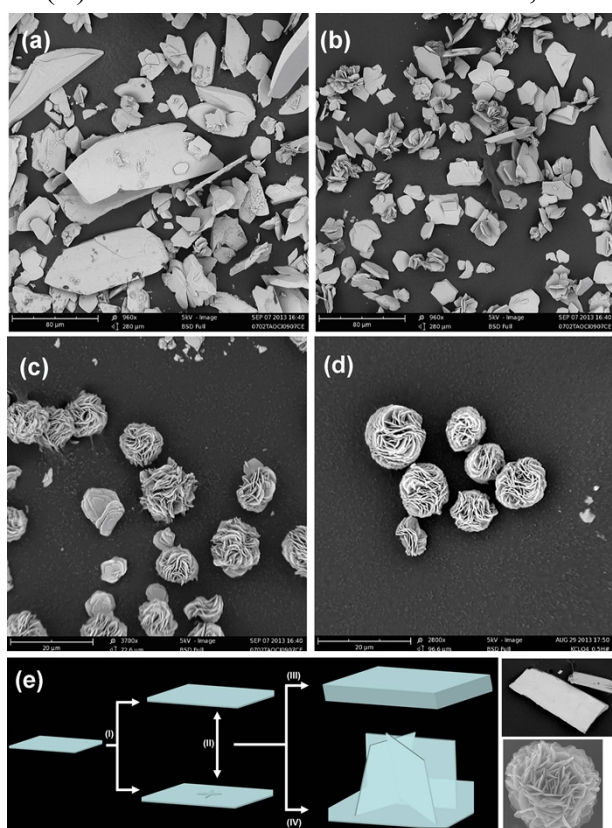
Figure S7. SEM images of **Ru-MOF** crystalline particles obtained in different reactant concentrations at 100℃ for 5h solvothermal reactions. (a) 5 equivalent, (b) 4 equivalent, (c) 3 equivalent and (d) 1 equivalent reactants at 10 mL DMF solution. The scale bars for (a), (b), (c) and (d) are 80 μm, 80 μm, 20 μm and 20 μm, respectively. And (e) the schematic illustration for the possible formation mechanism of bulk crystals and flower-like microspheres of **Ru-MOF**. The numbers (I)-(IV) in (e) represent the thermal fluctuations; equilibrium of spontaneous nucleation and dissipation; rapid crystallization and formation of flower-like microspheres.
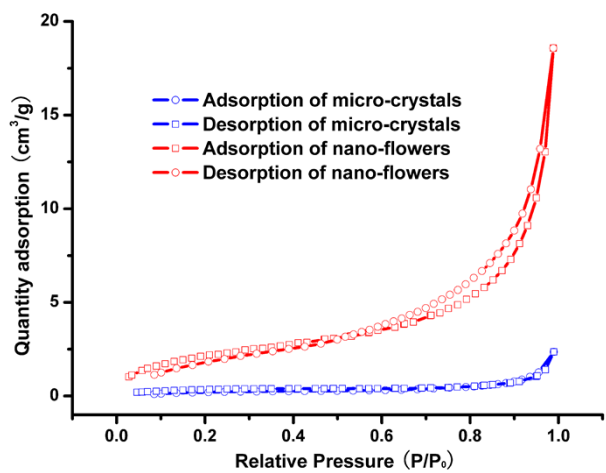
Figure S8. Nitrogen adsorption/desorption isotherm of nanoflowers and micro crystals of **Ru-MOF**.
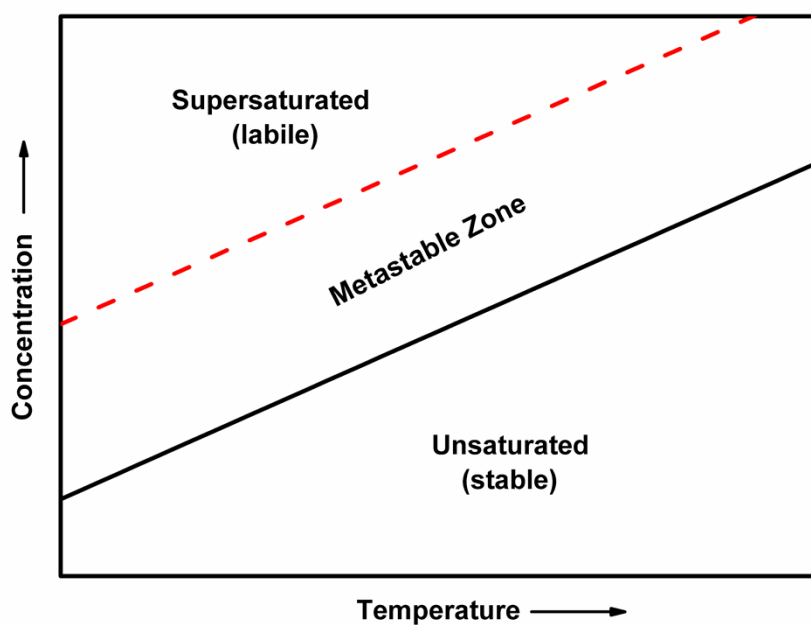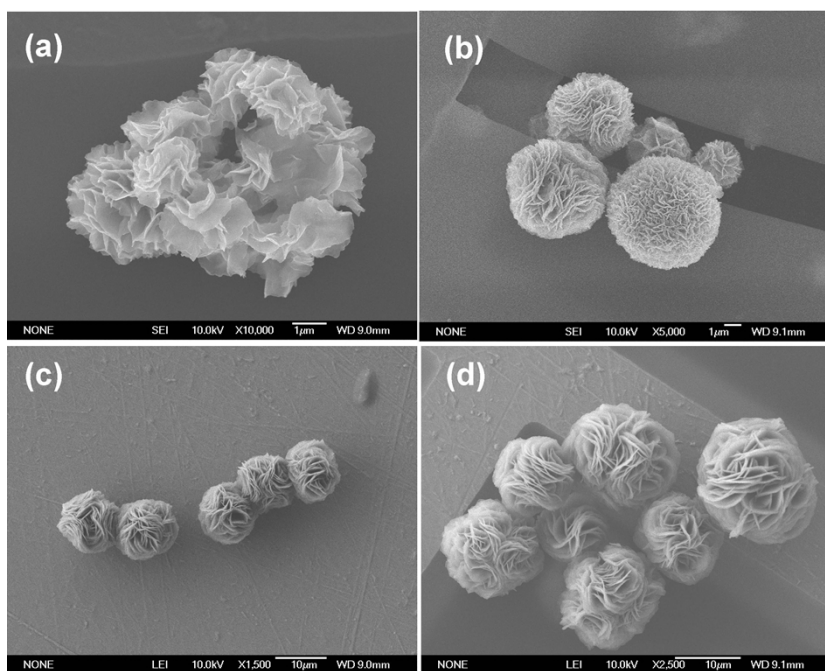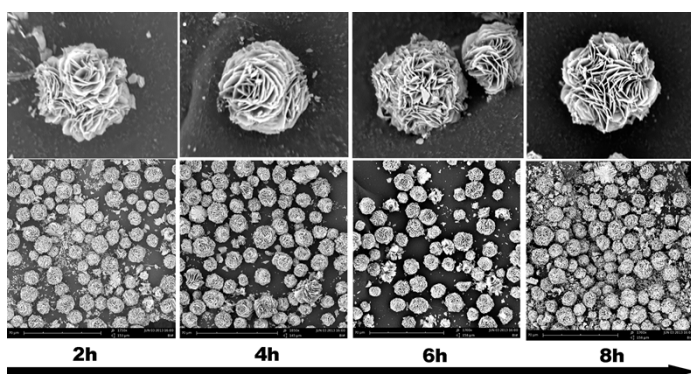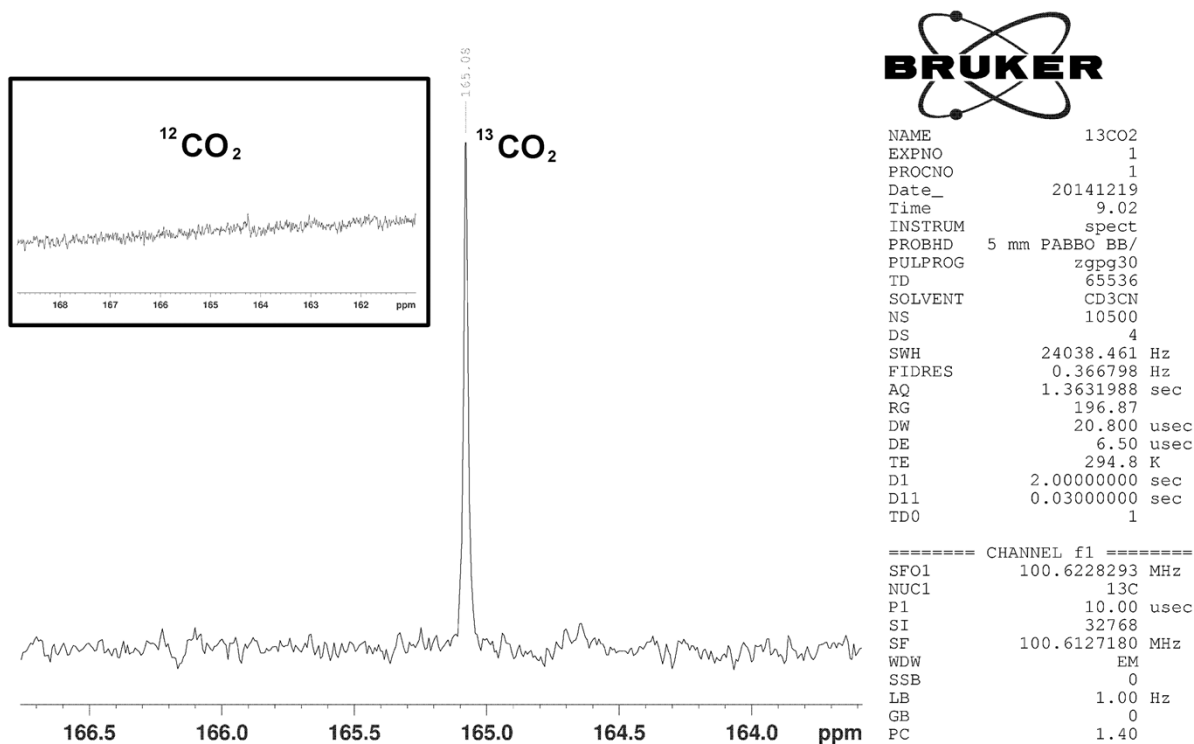

Figure S9. Schematic of solubility and saturation curves for **Ru-MOF** in the solution.

Figure S10. The morphology of the flower-like micro particles of **Ru-MOF** obtained under varied reaction time, (a) 1.5h, (b) 1.75h, (c) 2h and (d) 5h.


Figure S11. SEM images of flower-like microparticles after different photocatalytic reaction time.

Figure S12. The ^{13}C NMR spectra for the product obtained under the following reaction conditions: 4 mg photocatalyst, 6ml CD_3CN/TEOA (20:1 v/v), $^{13}CO_2$, 8h.
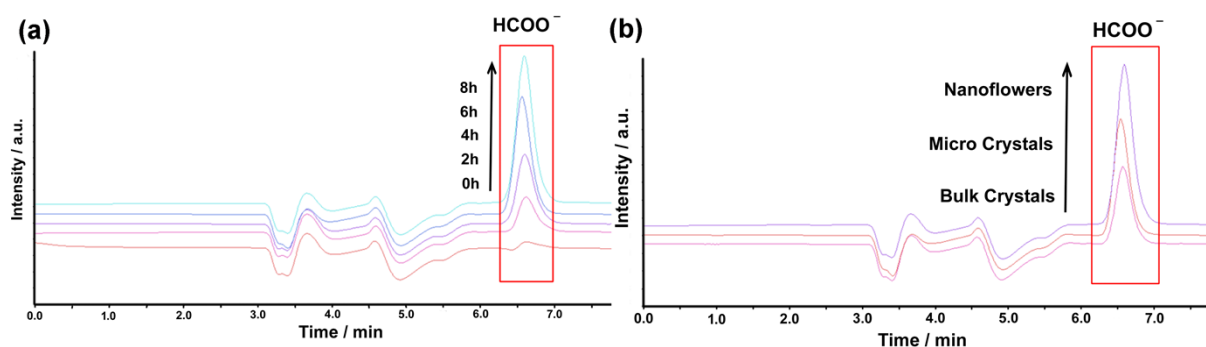
Figure S13. Ion chromatographic analyses of $HCOO^-$ on the products (a) after different photocatalytic reaction time. (b) generated by using different photocatalysts after 8 hours reactions.
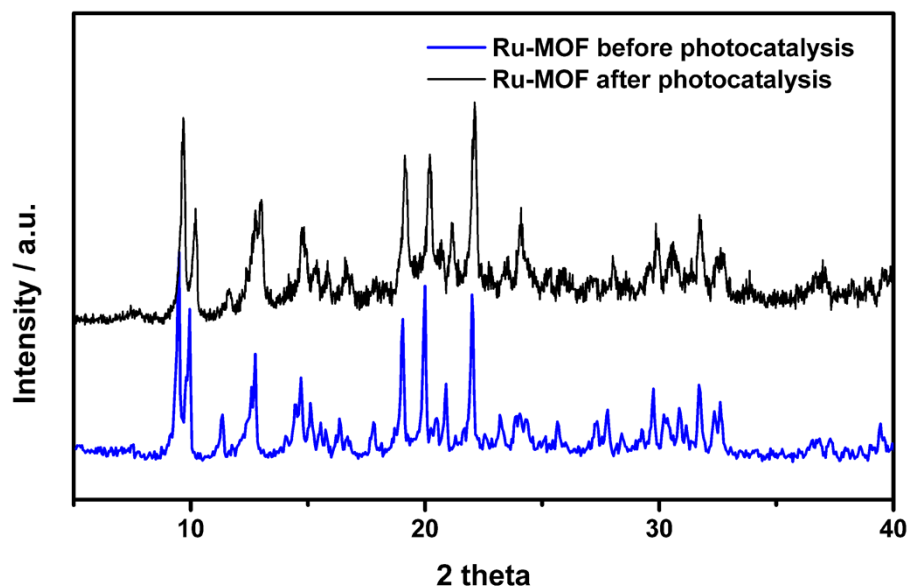
Figure S14. The PXRD patterns of Ru-MOF before and after photocatalytic reactions.
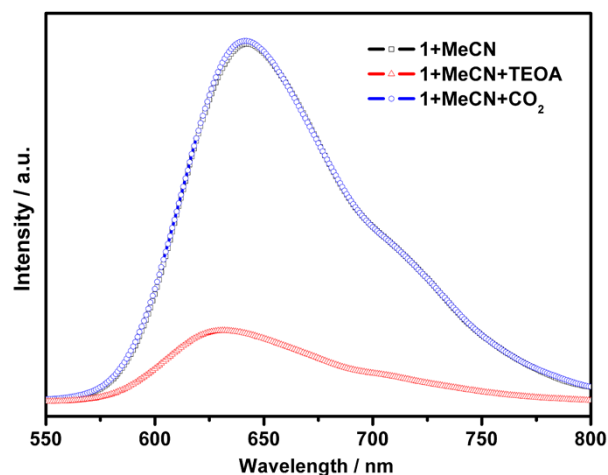
Figure S15. The luminescence nanoflowers dispersed in acetonitrile solution (black square) and with additional quenchers: TEOA (red triangle) and CO_2 (blue circle). The black square curve and blue circle curve are overlapped. The luminescence of nanoflowers was quenched by TEOA indicating the charge transfer from TEOA to Ru units.

Reference

1. E. Eskelinen, S. Luukkanen, M. Haukka, M. Ahlgrén and T. A. Pakkanen, *J. Chem. Soc., Dalton Trans.,* **2000**, 2745.
2. G. M. Sheldrick, SHELXS-97, Programs for X-ray Crystal Structure Solution. *University of Göttingen: Germany* **1997**.
3. A. L. Spek, PLATON, A Multipurpose Crystallographic Tool, *Utrecht University, Utrecht: The Netherlands* **2008**.
4. T. L. Hill, Thermodynamics of Small Systems; *Dover Publications: New York*, **1994**.
5. G. Ren, Z. Lin, B. Gilbert, J. Zhang, F. Huang and J. Liang, *Chem. Mater.* 2008, **20**, 2438.